

JPL Document D-64843

***TECHNOLOGY DEVELOPMENT FOR  
EXOPLANET MISSIONS***

*Technology Milestone White Paper  
Hybrid Lyot Coronagraph Technology – Linear Masks*

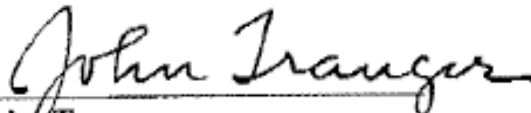
*John Trauger, P.I.  
Brian Gordon, John Krist, Dimitri Mawet,  
Dwight Moody, and Peggy Park*

***1 June 2010***

National Aeronautics and Space Administration  
Jet Propulsion Laboratory  
California Institute of Technology  
Pasadena, California

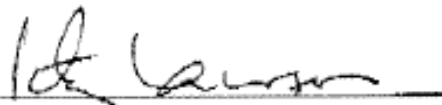
**Approvals:**

**Released by**

  
John Trauger  
Principal Investigator

6/8/2010  
Date

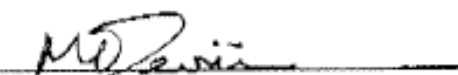
**Approved by**

  
Peter R. Lawson  
Exoplanet Program Technology Investigation Manager, JPL

6/11/2010  
Date

  
Marie Levine  
Exoplanet Program Technology Facilities Manager, JPL

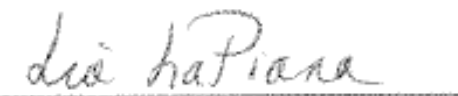
6/11/2010  
Date

  
Michael Devirian  
Exoplanet Exploration Program Manager, JPL

6/14/2010  
Date

  
Douglas Hudgins  
Exoplanet Exploration Program Scientist, NASA HQ

6/16/10  
Date

  
Lia LaPiana  
Exoplanet Exploration Program Executive, NASA HQ

6/14/10  
Date

# Table of Contents

<b>1. Objective .....</b>	<b>3</b>
<b>2. Introduction .....</b>	<b>3</b>
2.1. Relevance for a Future Exoplanet Mission .....	4
2.2. Hybrid Lyot Coronagraph Masks .....	5
2.3. HCIT configuration .....	6
2.4. Differences Between Flight and Laboratory Demonstrations .....	8
<b>3. Computation of the Metric .....</b>	<b>10</b>
3.1. Definitions .....	10
3.2. Measurement of the Star Brightness .....	12
3.3. Measurement of the Coronagraph Contrast Field .....	12
3.4. Milestone Demonstration Procedure .....	14
<b>4. Success Criteria .....</b>	<b>15</b>
<b>5. Certification .....</b>	<b>16</b>
<b>6. References .....</b>	<b>17</b>
<b>7. Appendix 1– Additional spectral bands.....</b>	<b>18</b>
<b>8. Appendix 2 – Stability of the HCIT .....</b>	<b>19</b>
<b>9. Appendix 3 – Overview of the ACCESS concept.....</b>	<b>21</b>

# **TDEM Milestone White Paper: Advanced Hybrid Lyot Coronagraph Technology**

## **1. Objective**

In support of NASA's Exoplanet Exploration Program and the ROSES Technology Development for Exoplanet Missions (TDEM), this whitepaper explains the purpose of the first TDEM Milestone for *Advanced Hybrid Lyot Coronagraph Technology*, specifies the methodology for computing the milestone metrics, and establishes the success criteria against which the milestone will be evaluated. This milestone is concerned with a demonstration of the hybrid mask in a linear form. A subsequent milestone is planned to demonstrate the same metrics for a hybrid mask of circular form.

## **2. Introduction**

TDEM Technology Milestones are intended to document progress in the development of key technologies for a space-based mission that would detect and characterize exoplanets, such as ACCESS (Trauger et al. 2008, 2009, 2010), thereby to gauge the mission concept's readiness to proceed from pre-Phase A to Phase A.

This milestone addresses broadband starlight suppression. We make reference to a space mission designed for high-contrast coronagraphic imaging in three discrete photometric bands spanning an overall 483–880 nm spectral range. The objective of this TDEM milestone is the validation of a new hybrid Lyot focal plane mask in a single 20% spectral band within that nominal range. A secondary goal extends the validation to two additional 20% bands, if resources allow, as described in Appendix 1.

The approach for this milestone builds upon that for TPF-C Milestones #1 and #2, which respectively demonstrated monochromatic and broadband (10%) starlight suppression in the High Contrast Imaging Testbed (HCIT). This milestone focuses on the validation of one key TDEM technology – the hybrid Lyot mask. It is more ambitious than the TPF-C Milestones in that a broader bandwidth is attempted. Success is defined in terms of statistically significant performance demonstrations of this key technology, ideally with minimal sensitivity or dependence on extraneous environmental factors.

Completion of this milestone is to be documented in a report by the Principal Investigator and reviewed by NASA HQ.

This milestone reads as follows:

### **Milestone definition:**

#### **Starlight Suppression with Linear Hybrid Lyot Masks**

*Demonstrate, using linear hybrid Lyot masks, calibrated coronagraph contrast of  $1 \times 10^{-9}$  at angular separations of  $3 \lambda_0 / D$  and greater in a single 720–880 nm (20%) spectral band.*

The width of the “spectral band” is defined as the ratio  $\delta\lambda/\lambda_0$ , where,  $\delta\lambda$  is the full width at half maximum (FWHM) transmittance of the band-defining optical filter and  $\lambda_0$  is the central wavelength. The “angular separation” and “inner and outer working angles” are defined in terms of the central wavelength  $\lambda_0$  and the diameter  $D$  of the aperture stop on the deformable mirror (DM), which is the pupil-defining element of the laboratory coronagraph. For this milestone, a hybrid mask will be fabricated with physical dimensions for a  $3\lambda_0/D$  inner working angle in an f/50 beam, corresponding to the current HCIT configuration with a 32-mm diameter pupil stop at the deformable mirror.

This milestone demonstration includes three specific criteria called out in the TDEM solicitation, as follows.

**(1) *Demonstration of milestone performance must be stable and repeatable, thereby demonstrating that the result is not spurious or transient.*** While the coronagraph mask technology is inherently stable, we will repeat the milestone demonstrations in order to build up statistical significance at the 90% confidence level, as further described in Section 3.1.7.

**(2) *Modeling of the milestone must be consistent with the demonstrated result, thereby establishing that the behavior is thoroughly understood.*** Optical models for testbed coronagraph performance have been developed by the investigation team. Our Fresnel propagation models incorporate the salient characteristics of the Lyot coronagraph elements, mirror surfaces, the deformable mirror, and the CCD imager. These models consistently predict laboratory contrast performance within ~15%, based on prior demonstrations on the HCIT, including TPF-C Milestones #1 and #2, and on further coronagraph demonstrations at 20% bandwidth in support of the ACCESS study.

**(3) *Error budget for the milestone must be consistent with the models.*** We rely on our optical models to predict the sensitivity of contrast performance to component imperfections, alignment errors, and sources of drift. The dominant terms in the error budget include the optical characteristics and location of the occulting mask, location of the Lyot stop, stability of the DM surface, and surface quality of the relay optics. For each term in the error budget, we compute the effects of the static error on the achievable contrast (using a standardized speckle nulling computation) and the sensitivity of the achieved contrast to drifts in that term absent further compensation by speckle nulling. A tolerance matrix that includes the error terms known to be most significant at the milestone contrast level (about 10 terms) will be compiled for this milestone report.

## **2.1. Relevance for a Future Exoplanet Mission**

Development of the hybrid Lyot technology is intended to advance the readiness of a mission concept for the coronagraphic imaging and spectroscopic observation of exoplanetary systems. ACCESS serves as a representative probe-class mission concept. Attached as Appendix 3, a recent paper provides a brief overview of the ACCESS concept. A more detailed description can be found in the 176-page ACCESS final report to NASA (Trauger et al. 2009).

To detect exoplanets in the super-Earth to Jovian range, a coronagraph must provide raw image contrast of  $10^{-9}$  in a dark field near the parent star. It is expected that post-processing of coronagraph data will provide detection sensitivities to planets and debris

disks an order of magnitude fainter (Trauger and Traub 2007). Therefore, this milestone requires a demonstration of a high contrast dark field at the  $10^{-9}$  level.

ACCESS forms a high contrast “dark field” over a working angle spanning  $3\text{--}24 \lambda_0 / D$ . The inner working angle ( $3 \lambda_0 / D$ ) is defined by science requirements, while the outer working angle ( $24 \lambda_0 / D$ ) is defined by the highest spatial frequency controlled by a deformable mirror (DM) with 48 actuators across the pupil diameter  $D$ . Extensive optical modeling and tolerancing has shown that it is increasingly difficult to control the contrast in the dark field as one moves closer to the image of the target star. This milestone addresses the most challenging location in the image plane, the inner working angle at the same angular separation as will be required by ACCESS. The HCIT DM has 1024 actuators controlling the surface of a  $32 \times 32$  mm mirror facesheet. This is fewer actuators than presumed for ACCESS, so this milestone addresses a smaller outer working angle (out to  $10 \lambda_0 / D$ ). This is of sufficiently large size that the physics of the wavefront control problem can be demonstrated with high expectation of applying the same approach to a larger dark field at a later date. The outer working angle for the flight mission is achieved using a DM with more actuators.

The contrast specification relates to the average contrast level in the dark field of interest around the source or parent star. This criterion was used in TPF-C milestones #1 and #2. It should be applicable to any coronagraph that propagates its image from sky to the coronagraph focal plane without optical distortions. Analysis of contrast in the dark field must necessarily account for the statistical nature of the static and “quasi-static” speckle patterns. Speckle analysis is further complicated by the systematic evolution of the speckle patterns by wavelength over the 20% spectral band, as well as the deterministic effects of wavefront control using a deformable mirror. The milestone measurements themselves will result in a distribution of speckle intensities, from which we will estimate the average contrast and statistical confidence levels. Statistical measures of both the average intensity and its variance in the coronagraph dark field will be provided in support of the milestone validation package, as specified in Section 5 below.

## 2.2. Hybrid Lyot Coronagraph Masks

Among the four major coronagraph types studied by ACCESS, the hybrid Lyot coronagraph represents the highest readiness level, having demonstrated the best laboratory contrast and bandwidth to date, thereby providing the most reliable estimate of science performance available with today’s technology, as well as providing a solid basis for determination of mission cost, risk, and schedule.

For a mask design with a single thickness-profiled metallic layer, the earlier approach had been to create an attenuation profile with a prescribed “band limited” form (Kuchner and Traub 2002), while accepting without change the resulting phase shifts that necessarily accompany the attenuation in real materials (as in Figure 1). In general, such “parasitic” phase shifts violate the criteria for band-limited coronagraph masks, and further, these materials may exhibit significant dispersion in optical properties over spectral bandwidths ( $\delta\lambda/\lambda_0 = 20\%$ ) that are of interest for exoplanet astronomy (Moody and Trauger 2007, Balasubramanian 2008). The hybrid approach provides a measure of control over phase by adding a thickness-profiled non-absorbing dielectric layer (Moody et al. 2008). These hybrid Lyot masks are composed of metal and dielectric layers superimposed as a multilayer coating on a glass substrate.

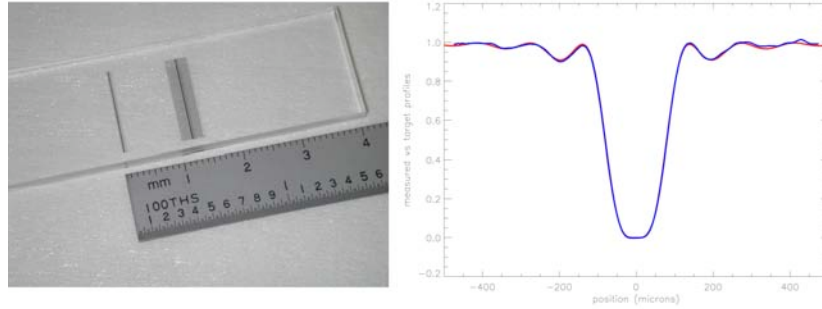


**Figure 1.** An example of a linear Lyot focal plane coronagraph mask (Moody and Trauger 2007). At left, a 4th order nickel-only mask deposited on a fused silica substrate. At right, a comparison between the desired profile (red) and the measured profile (blue).

The mask design process will be upgraded to facilitate a more optimal solution to the non-linear problem of speckle suppression over a range of wavelengths, where design parameters include the gamut of physically realizable mask profiles and the range of allowed actuator settings on a deformable mirror. Our thin film interference code (which generates thin film multilayer thickness profiles to match specified attenuation and phase profiles) will be integrated with our wavefront control optimization code (which finds the optimal settings for the deformable mirror in the context of a realistic coronagraph) in order to more effectively search for the optimal spectrally-broad design. We will consider deviations from the standard 4<sup>th</sup> order apodization profiles for a more effective balance between high contrast at small working angles and overall throughput.

On the fabrication side, the proposed work will modify and refine the existing deposition system for improved fidelity of the manufactured profile. We will explore a number of new materials for the hybrid masks. The optical density and phase shift profiles of the fabricated masks will be characterized in detail in our laboratory.

### 2.3. HCIT configuration

The current optical layout of the HCIT Lyot table is shown in the Figure 2, taken from Trauger et al. (2007). The optical system resides in a vacuum chamber that can be evacuated to  $\sim 10$  milliTorr levels. Minor modifications to this configuration will likely be required to accommodate the various TDEM demonstrations scheduled to take place on this table.

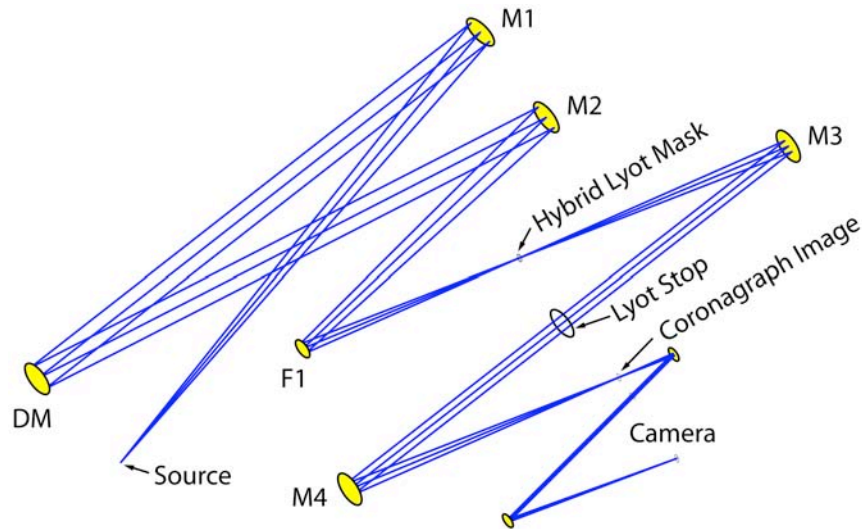


**Figure 2.** *Optical layout of the HCIT Lyot coronagraph table. The optical elements, in the optical path starting from the source, are as follows. The source of continuum light illuminates M1, the first of six off-axis paraboloidal (OAP) mirrors, where the beam is collimated. The beam passes to the deformable mirror (DM), where an aperture stop defines the pupil of the system. The DM is from Xinetics, with 1024 actuators driving a mirror facesheet measuring 32×32 mm. The collimated light is then focused by M2 and folded by the flat mirror F1, passing to the focal plane where the hybrid Lyot mask will be located. The beam is then collimated by M3 on its way to the Lyot stop, which is located in a pupil plane conjugate to the deformable mirror. The collimated beam is then brought to a focus by M4 to create the high-contrast coronagraph image, as indicated. A camera, formed by a pair of small OAPs, then magnifies and projects the coronagraph image onto the CCD focal plane.*

The milestone demonstration will rely on a wavefront sensing and correction process that has been validated in previous milestone demonstrations, including TPF-C Milestone #2. A flavor of the “electric field conjugation method” (EFC), as described in Give’on *et al.* (2007), is used and iterated repeatedly as necessary, as follows. For each filter in a set of three optical filters with contiguous 7% passbands that discretely sample the full 20% range of wavelengths, and starting with a nominally flat surface figure setting on the DM: (a) take the set of contrast field images with the initial DM setting and estimate the contrast averaged across the entire 20% band; (b) take images for each of four “probe” DM settings (consisting of small deterministic surface figure deviations from the initial DM setting) to estimate of the effects of the four probe settings across the entire 20% band; (c) use these data to compute the complex electric field in the target dark field region across the 20% band; and then (d) calculate and apply a new DM setting that will reduce the energy over the dark field in all filters concurrently, thus establishing a new “initial DM setting” in preparation for the next iteration, which is a loop back to step (a). A typical integration time for an individual image is about ten seconds, and one complete wavefront sensing and control cycle, including overhead for CCD readouts, data handling and computations for a 20% band, typically takes 10-15 minutes.

## 2.4. Differences Between Flight and Laboratory Demonstrations

There are several important differences between the lab demonstration and the ACCESS flight implementation. Each is addressed briefly below

**Starlight:** In a space coronagraph, the spectrum of light illuminating the coronagraph would closely resemble black body radiation. In practice, the spectral distribution produced by the HCIT light source (a fiber-coupled supercontinuum laser) is smooth across a 20% spectral band, with brightness vs. wavelength that can be described by a second order polynomial  $f(\lambda)=a+b\lambda+c\lambda^2$ . This is illustrated in Figure 3, an example in which greater intensity is received at the longer wavelengths, biasing the average contrast if it were estimated with a single 10% bandpass filter. We note that a further complication is introduced by the need to couple the supercontinuum radiation into an optical fiber that feeds light to the coronagraph, where drifts in the alignment between the supercontinuum output fiber and the input fiber leading to the coronagraph can produce a slowly time-varying modulation of the spectral shape of the light reaching the coronagraph.

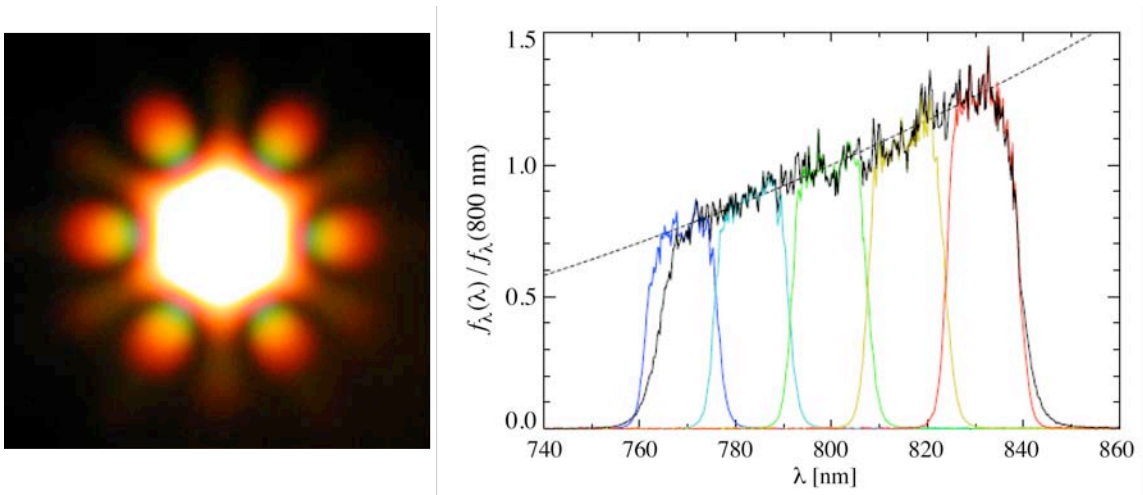


**Figure 3.** At left, the spectral content in the far-field output from a photonic crystal fiber, which leads to a correlation between source alignment and supercontinuum spectrum. At right, the construction of the 20% spectrum from a series of narrower filters. This example, taken from TPF-C Milestone #2 (Kern et al. 2008), compares spectra of the supercontinuum source transmitted by five 2% filters (in color) and a single 10% filter (in black). The dotted line traces the unfiltered output from the supercontinuum lamp. Average contrast over the full passband is estimated from contrast measurements taken in each of the narrow filters. Note that for this milestone, unlike the illustrated case, a set of three 7% filters with contiguous passbands will be used to represent the full 20% spectral band.

As such, a single filter spanning a 20% spectral band will not provide a reliable test of the contrast over the entire spectral band. Instead, the contrast will be measured in a set of three contiguous 7% passbands that cover the full 20% band. The measurements in each 7% band are individually calibrated against the photometry reference (as described in Section 3.3) and averaged to construct the contrast metric over the full 20% spectral band. The three filters are mounted in a wheel outside the vacuum chamber, so that they

can be interchanged easily without disrupting the optical system in any way. This procedure effectively corrects for the shape  $f(\lambda)$ , as long as the time scale for variations is long compared to the time for one wavefront sensing and control iteration.

The supercontinuum source provides a photon flux that is comparable to or somewhat brighter than the target stars to be observed by the mission (e.g., a star with visual magnitude  $V=1$  observed with a 1.5 meter telescope). The goal of this milestone is to demonstrate the broadband contrast that can be achieved, which is independent of the source intensity, so a bright source is a convenience that does not compromise the integrity of the demonstration.

Finally, unlike the light collected by a telescope from a target star, the light intensity is not uniform across the pupil. Typically this non-uniformity is a center-to-edge “droop” of a few percent corresponding to the diffraction pattern from a small pinhole. This small level of non-uniformity has negligible effect on the final contrast if it is accounted for in the wavefront control algorithm, and would result in a finite but below-requirement loss of contrast if it were ignored in the control algorithm.

**Spacecraft dynamics:** A control system is required in flight to stabilize the light path against motions of the spacecraft. The dominant effects of spacecraft dynamics are jitter of the star image on the coronagraph focal plane mask and beam walk in the optics upstream of the focal plane mask. For a specific example, the ACCESS analysis showed that for fourth-order coronagraphs (including Lyot, vortex, and pupil mapping coronagraphs) with an inner working angle of  $3\lambda_0/D$ , that pointing errors needed to be less than  $\pm 0.03 \lambda_0/D$  to limit the corresponding contrast degradation to less than  $2 \times 10^{-10}$ . The concept models have shown that the required pointing stability can be achieved in space with current high Technology Readiness Level (TRL) systems. Scaled to the HCIT, this would correspond to an ability to center the occulting mask on the “star” within 1  $\mu\text{m}$ , or about 0.23 pixel when projected to the CCD focal plane (Appendix 2).

The milestone demonstration requires the passive stability of the testbed, including the centration of the star on the occulter as one example, which is untraceable to spacecraft dynamics. In practice, the HCIT often exhibits alignment drifts that are larger than expected in the space environment. As such we must rely on favorable periods of thermal and mechanical stability of the HCIT.

**Single deformable mirror:** The milestone demonstrations will be carried out with a single DM, which allows the control of phase and amplitude in the complex wavefront over one half of the coronagraph field described in Section 2 above. In flight, it is expected that a pair of DMs will be used, in series, to generate a full (two-sided) dark field, with the added advantages of a deeper contrast field and better broadband control.

## 3. Computation of the Metric

### 3.1. Definitions

The contrast metric requires a measurement of the intensity of speckles appearing within the dark field, relative to the intensity of the incident star. The contrast metric will be assessed in terms of statistical confidence to capture the impact of experimental noise and uncertainties. In the following paragraphs we define the terms involved in this process, spell out the measurement steps, and specify the data products.

**3.1.1.** “Raw” Image and “Calibrated” Image. Standard techniques for the acquisition of CCD images are used. We define a “raw” image to be the pixel-by-pixel image obtained by reading the charge from each pixel of the CCD, amplifying and sending it to an analog-to-digital converter. We define a “calibrated” image to be a raw image that has had background bias subtracted and the detector responsivity normalized by dividing by a flat-field image. Saturated images are avoided in order to avoid the confusion of CCD blooming and other potential CCD nonlinearities. All raw images are permanently archived and available for later analysis.

**3.1.2.** We define “scratch” to be a DM setting in which actuators are set to a predetermined surface figure that is approximately flat (typically, about 20 volts on each actuator).

**3.1.3.** We define the “star” to be a small pinhole illuminated with broadband light relayed via optical fiber from a source outside the HCIT vacuum wall (e.g., the super-continuum white light source). The “small” pinhole is to be unresolved by the optical system; e.g., a 5- $\mu\text{m}$  diameter pinhole would be “small” and unresolved by the 40- $\mu\text{m}$  FWHM Airy disk in an  $f/50$  beam at 800 nm wavelength. This “star” is the only source of light in the optical path of the HCIT. It is a stand-in for the star image that would have been formed by a telescope system.

**3.1.4.** We define the “algorithm” to be the computer code that takes as input the measured speckle field image, and produces as output a voltage value to be applied to each element of the DM, with the goal of reducing the intensity of speckles.

**3.1.5.** The “contrast field” is a dimensionless map representing, for each pixel of the detector, the ratio of its value to the value of the peak of the central PSF that would be measured in the same testbed conditions (light source, exposure time, Lyot stop, etc.) if the coronagraph focal plane mask were removed. The calibration of the contrast field is further detailed in Section 3.3.

**3.1.6.** The “contrast value” is a dimensionless quantity that is the average value of the contrast field over the dark field adopted for the experiment.

**3.1.7.** “Statistical Confidence”. The interpretation of measured numerical contrast values shall take into consideration, in an appropriate way, the statistics of measurement, including detector read noise, photon counting noise, and dark noise.

The milestone objective is to demonstrate with high confidence that the true contrast value in the dark field, as estimated from our measurements, is equal to or better than the required threshold contrast value  $C_\theta$ . The estimated true contrast value shall be obtained

from the average of the set of four or more contrast values measured in a continuous sequence (over an expected period of approximately one hour or more).

For this milestone the required threshold is a mean contrast value of  $C_0 = 1.0 \times 10^{-9}$  with a confidence coefficient of 0.90 or better. Estimation of this statistical confidence level requires an estimation of variances. Given that our speckle fields contain a mix of static and quasi-static speckles (the residual speckle field remaining after the completion of a wavefront sensing and control cycle, together with the effects of alignment drift following the control cycle), that they include the superposition of speckles of multiple wavelengths exhibiting their own deterministic wavelength dependencies, as well as other sources of measurement noise including photon detection statistics and CCD read noise, an analytical development of speckle statistics is impractical. Our approach is to compute the confidence coefficients on the assumption of Gaussian statistics, but also to make the full set of measurement available to enable computation of the confidence levels for other statistics. One data product will be a goodness of fit of the measurement with a normal distribution (Kolmogorov-Smirnov test).

At any time in the demonstration, the true contrast is subject to laboratory conditions, including the quality of the optical components, their alignment, any drift in their alignment over time, and the effectiveness of each wavefront sensing and control cycle. With each iteration, our nulling procedure attempts to improve the contrast value, thus compensating for any drift or changes in alignment that may have occurred since the previous iteration, and further variations may be expected due to experimental noise and any limitations in the algorithm. The data set built up from a sequence of such iterations will provide a distribution of contrast values, which will be regarded as Gaussian about a mean contrast for the data set. We therefore consider the mean contrast value as representative of the true contrast value for a data set, and the distribution of contrast determinations among the iterations within the data set as a combination of both random wavefront control errors and random measurement errors.

The mean contrast values and confidence limits are computed in the following manner. The average of one or more images taken at the completion of each iteration is used to compute the contrast value  $c_i$ . The mean contrast for a set of images taken in a given sequence is:

$$\hat{c} = \sum_{i=1}^n \frac{c_i}{n}$$

where  $n$  is the number of images in each set. The standard deviation  $\sigma_{each}$  in the contrast values  $c_i$  obtained for individual images within the set, which now includes both the measurement noise and the (assumed random) contrast variations due to changes in the DM settings for each speckle nulling iteration, is:

$$\sigma_{each} = \sqrt{\sum_{i=1}^n \frac{(c_i - \hat{c})^2}{n-1}}$$

Our estimate  $\hat{c}$  is subject to uncertainty in the contrast measurements  $\sigma_{mean} = \sigma_{each} / \sqrt{n}$  and the independently-determined overall errors in photometry  $\sigma_{phot}$ . With the approximation that the contrast values have a Gaussian distribution about the mean

contrast, then the statistical confidence that the mean contrast is less than  $C_0 = 1 \times 10^{-9}$  is given by:

$$conf = \frac{1}{\sqrt{2\pi}} \int_{-\infty}^t e^{-z^2/2} dz$$

where  $t = (C_0 - \hat{c}) / \sigma$  and  $\sigma = \sqrt{\sigma_{mean}^2 + \sigma_{phot}^2}$ . The values  $\hat{c}$  and  $\sigma$  are the milestone metrics. The 90% confidence value is the value  $C_0$  such that  $conf(C_0) = 0.9$  according to the above equations.

## 3.2. Measurement of the Star Brightness

The brightness of the star is measured with the following steps.

**3.2.1.** The occulting mask is laterally offset, so as to place a transparent region in its transmittance profile at the location of the star image. The transmittance profile of the occulting mask is known from imaging data from a microscope CCD camera.

**3.2.2.** To create the photometric reference, a representative sample of short-exposure (e.g. a few milliseconds) images of the star is taken, with all coronagraph elements other than focal-plane occulting mask in place.

**3.2.3.** The images are averaged to produce a single star image. The “short-exposure peak value” of the star’s intensity is estimated. Since the star image is well-sampled in the CCD focal plane (the Airy disk is sampled by  $\sim 20$  pixels within a radius equal to the FWHM), the star intensity can be estimated using either the value of the maximum-brightness pixel or an interpolated value representative of the apparent peak.

**3.2.4.** The “peak count rate” (counts/sec) is measured for exposure times of microseconds to tens of seconds.

## 3.3. Measurement of the Coronagraph Contrast Field

Each “coronagraph contrast field” is obtained as follows:

**3.3.1.** The occulting mask is centered on the star image.

**3.3.2.** An image (typically exposure times of  $\sim$ tens of seconds) is taken of the coronagraph field (the suppressed star and surrounding speckle field). The dimensions of the target areas, as shown schematically in Figure 4, are defined as follows: (a) A dark outer (D-shaped) field extending from 3 to  $10 \lambda_0/D$ , representing a useful search space, is bounded by a straight line that passes  $3 \lambda_0/D$  from the star at its closest point, and by a circle of radius  $10 \lambda_0/D$  centered on the star. (b) An inner area within the foregoing dark field, representing contrast at the inner working angle of  $3 \lambda_0/D$ , is bounded by a square box, each side measuring  $\lambda_0/D$ , such that one side is coincident with the foregoing straight line and centered on the closest point to the star.

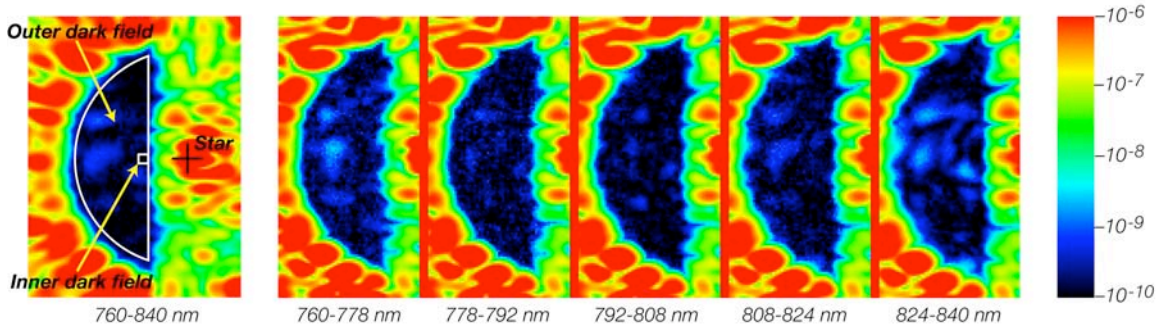


**Figure 4.** Definition of the high-contrast dark field. As described in the text, inner and outer regions are defined for the one-sided dark field. The location of the suppressed central star is also indicated. Adapted from Moody *et al.* (2008), this shows the dark field averaged over a 10% bandwidth (at left), and the five individual 2% dark fields (at right), corresponding to the TPF-C Milestone 2 demonstration.

**3.3.3.** The image is corrected for the attenuation profile of the occulter and normalized to the “star brightness” as defined in 3.2. For this purpose, the fixed relationship between peak star brightness and the integrated light in the speckle field outside the central DM-controlled area will be established, as indicated in Figure 5 (taken from TPF-C Milestone Report #1, Trauger *et al.* 2006), providing the basis for estimation of star brightness associated with each coronagraph image.

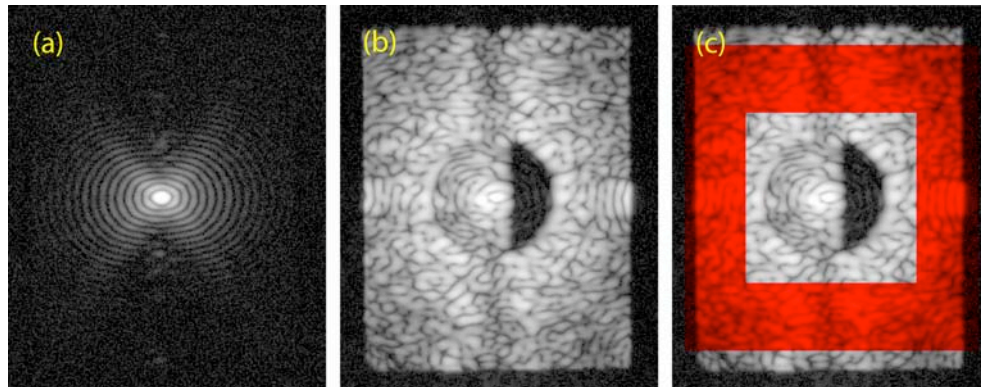


**Figure 5.** Reference fields for contrast photometry. Shown here are (a) the “planet” reference image; (b) the high-contrast coronagraph field; and (c) superimposed in red is the reference speckle field in the “uncontrolled” area beyond the Nyquist limit for the deformable mirror. Images are displayed with a logarithmic contrast stretch.

**3.3.4.** The contrast field image is averaged over the target high-contrast areas, to produce the contrast value. To be explicit, the contrast value is the sum of all contrast values, computed pixel-by-pixel in the dark field area, divided by the total number of pixels in the dark field area, without any weighting being applied. The rms contrast in a given area can also be calculated from the contrast field image.

### **3.4. Milestone Demonstration Procedure**

The procedure for the milestone demonstration is as follows:

**3.4.1.** A set of three 7% FWHM filters are used to represent the 20% spectral band. The DM is set to scratch. An initial coronagraph contrast field image is obtained for each of the three filters, as described in Sec. 3.3.

**3.4.2.** Wavefront sensing and control is performed to find settings of the DM actuators that give the required high-contrast across the 20% band in the target dark field. This iterative procedure may take from one to several hours, starting from scratch, if no prior information is available. However it can take more or less time depending on the stability of the HCIT optical system.

**3.4.3.** Subsequent contrast field images are taken, in each of the three filters, following steps 3.3.1 – 3.3.4, at the rate of about four contrast field images per hour, for a period of at least one hour. The result at this point is a set of contrast field images covering the 20% spectral band. It is required that a sufficient number of images are taken to provide statistical confidence that the milestone contrast levels have been achieved, as described in Section 3.1.7 above.

**3.4.4.** Laboratory data are archived for future reference, including raw and calibrated images of the reference star and contrast field images.

## 4. Success Criteria

The following are the required elements of the milestone demonstration. Each element includes a brief rationale.

**4.1.** A set of three optical filters, with contiguous 7% passbands, shall be used to discretely sample the 720–880 nm (20%) FWHM wavelength range. Contrast values for each of these filters shall be averaged to determine the broadband contrast.

*Rationale: As described in Section 2.3, this approach is required to correct for spectral variations in the supercontinuum light source, a problem that will not be encountered with real stars in a space mission.*

**4.2.** A mean contrast metric of  $1 \times 10^{-9}$  or better shall be achieved in both an outer target dark area ranging from 3 to  $10 \lambda_0/D$  and an inner area ranging from 3 to  $4 \lambda_0/D$ , as defined in Sec. 3.3.2.

*Rationale: The outer area provides evidence that the high contrast field provides a useful search space for planets. The inner area tests for fundamental limitations at the inner working angle.*

**4.3.** Criteria 4.1 and 4.2, averaged over the data set, shall be met with a confidence of 90% or better, as defined in Sec. 3.1.7. Sufficient data shall be taken to justify this statistical confidence. It is expected that this confidence level can be met with a data set taken as a single sequence of images over a period of one hour or more. This criterion is deemed to have been met by a data set exhibiting the stated statistical confidence.

*Rationale: This milestone is intended to validate the ability of the hybrid mask technology to deliver the contrast and bandwidth performance specified in Section 2. The mask itself is a passive element of the coronagraph, constructed with the same methods and materials used for optical filters that have flown in space for decades, with optical characteristics that can be considered permanent and insensitive to the environmental influences of a space mission. As such, a statistically significant measurement of achieved coronagraph contrast establishes the capability of the mask.*

**4.4** The demonstration described in 4.3 will be repeated on three separate occasions, with different masks used on each occasion. In this context a different mask is deemed to be either a different section of a linear mask separated by an angle of at least  $3 \lambda_0/D$ , or a physically separate mask.

*Rationale: Because the milestone is directed at a component test, the component must change between tests, but it is not required that the software control system be reset between each demonstration. This is to say that for each demonstration, the DM need not begin from a “scratch” setting and the DM control algorithm may retain memory of settings used for prior demonstrations. There is no time requirement for the demonstrations, other than the time required to meet the statistics stipulated in success criterion 4.3. There is no required interval between demonstrations. Subsequent demonstrations can begin as soon as prior demonstration has ended. There is no requirement to turn off power, open the vacuum tank, or delete data relevant for the calibration of the DM response functions.*

## 5. Certification

The PI will assemble a milestone certification data package for review by the ExEPTAC and the ExEP program. In the event of a consensus determination that the success criteria have been met, the project will submit the findings of the review board, together with the certification data package, to NASA HQ for official certification of milestone compliance. In the event of a disagreement between the ExEP project and the ExEPTAC, NASA HQ will determine whether to accept the data package and certify compliance or request additional work.

### 5.1. Milestone Certification Data Package

The milestone certification data package will contain the following explanations, charts, and data products.

- 5.1.1.** A narrative report, including a discussion of how each element of the milestone was met, and a narrative summary of the overall milestone achievement.
- 5.1.2.** A description of the optical elements and their significant characteristics.
- 5.1.3.** A tabulation of the significant operating parameters of the apparatus.
- 5.1.4.** A calibrated image of the reference star, and the photometry method used.
- 5.1.5.** Calibrated images of the Lyot mask transmittance pattern.
- 5.1.6.** Spectrum of the broadband light and an estimate of the intensity uniformity of the illumination reaching the defining pupil (at the DM).
- 5.1.7.** A contrast field image representative of the data set, with appropriate numerical contrast values indicated, with coordinate scales indicated in units of Airy distance ( $\lambda_0/D$ ).
- 5.1.8.** A description of the data reduction algorithms, in sufficient detail to guide an independent analysis of the delivered data.
- 5.1.9.** Contrast metric values and supporting statistics for the overall data used to satisfy the milestone requirements, including a pixel-by-pixel histogram of contrast values across the dark field.

## 6. References

- Balasubramanian, K., “Materials for band-limited image plane masks”, *Appl. Opt.* **47**, 116, 2008.
- Give’on, A., B. Kern, S. Shaklan, D. Moody, and L. Pueyo, “Broadband wavefront correction algorithm for high-contrast imaging systems,” *Proc. SPIE* **6691**, 66910A, 2007.
- Kern, B. *et al.*, “TPF-C Milestone #2 Report,” JPL Document D-60951, August 2008.
- Kuchner, M., and W. Traub, “A coronagraph with a band-limited mask for finding terrestrial planets,” *Astrophys. J.* **570**, 900, 2002.
- Moody, D., B.L. Gordon, and J. Trauger, “Design and demonstration of hybrid Lyot coronagraph masks for improved spectral bandwidth and throughput,” *Proc. SPIE* **7010**, 70103P, 2008.
- Trauger, J. *et al.*, “TPF-C Milestone #1 Report,” JPL Document D-35484, July 2006.
- Trauger, J. and W. Traub, “A laboratory demonstration of the capability to image an Earth-like extrasolar planet,” *Nature* **446**, 771, 2007.
- Trauger, J., A. Give’on, B. Gordon. B. Kern, A. Kuhnert, D. Moody, A. Niessner, F. Shi, D. Wilson, and C. Burrows, “Laboratory demonstrations of high-contrast imaging for space coronagraphy,” *Proc. SPIE* **6693**, 66930X, 2007.
- Trauger, J. *et al.*, “ACCESS – A NASA mission concept study of an Actively Corrected Coronagraph for Exoplanet System Studies,” *Proc. SPIE* **7010**, 701029, 2008.
- Trauger, J. *et al.*, “ACCESS – A space coronagraph concept for direct imaging and spectroscopy of exoplanetary systems,” Public version of the Final Report to the NASA Astrophysics Strategic Concept Studies Program, April 2009.
- Trauger, J. *et al.*, “ACCESS – A Concept Study for the Direct Imaging and Spectroscopy of Exoplanetary Systems,” *Pathways towards Habitable Planets, ASP Conf. Series*, 2010.

## 7. Appendix 1– Additional spectral bands

Previous demonstrations on the HCIT Lyot Table have been confined to the 720–880 nm spectral range. An objective of the Hybrid Lyot TDEM proposal is the validation of milestone-level contrast in each of three 20% passbands (483–590, 590–720, and 720–880 nm) that span an overall 483–880 nm spectral range. Such a demonstration requires a number of modest modifications to the Lyot Table as currently configured. However, it is unknown at the time of this writing whether these modifications are within the scope of the TDEM program, as must be determined in consultation with the Technology Facilities Manager. Further, it needs to be established that these facility modifications would be acceptable to all TDEM PIs planning to use the Lyot Table, as must be determined in consultation with the Community Users Group.

The modifications needed to accommodate additional spectral bands are listed here.

- 1) **Mirror coatings:** Currently all HCIT mirrors are coated with bare gold, which provides acceptable reflectance only for the longest (720–880 nm) of the three specified spectral bands. For demonstrations in the two additional spectral bands (483–590 and 590–720 nm), a suitable alternative is required that provides useful reflectance over the entire 483–880 nm spectral range. Aluminum is the preferred alternative mirror coating, since it offers the minimal potential for extraneous polarization or dispersive phase shifts. Recoating the optics involves down-time of approximately one month for the mirror coating and the remounting and realignment of the optical elements.
- 2) **Antireflection coatings:** The fused silica window of the CCD camera needs an antireflection coating appropriate for the full spectral band.
- 3) **Supercontinuum lamp:** In all previous HCIT experiments, the spectral coverage has been restricted to wavelengths within the range 720–880 nm. The additional spectral bands require light source that covers the 483–880 nm wavelength range. There are two such lamps in the HCIT inventory. Measurements are needed to verify that their output spectra extend over the entire wavelength range.
- 4) **Additional spectral filters:** Accommodation of additional spectral filters (as described in Section 2.3) to cover the 483–590 and 590–720 nm bands. This involves the purchase of additional optical filters, filter selection mechanisms, and minor software adjustments.

An investigation of the Hybrid Lyot coronagraph contrast for the 483–590 and 590–720 nm bands would be implemented under the following guidelines.

- 1) These demonstrations shall be attempted only after the objectives of the Milestone have been completed.
- 2) They are contingent on the completion of modifications 1–4 listed above.
- 3) They would be carried out with the same Lyot Table setup and within the experiment time scheduled for this milestone demonstration.

## 8. Appendix 2 – Stability of the HCIT

Here we illustrate one of the dominant stability requirements for the ACCESS flight mission, then borrow the analysis to estimate laboratory stability requirements for the hybrid Lyot contrast milestone. We then relate this requirement to the typical stability of the HCIT.

A control system is required in flight to stabilize the light path against motions of the spacecraft. The dominant effects of spacecraft dynamics are jitter of the star image on the coronagraph focal plane mask and beam walk in the optics upstream of the focal plane mask. For a specific example, shown in Figure 3-1, the ACCESS analysis showed that for fourth-order coronagraphs (including Lyot, vector vortex, and pupil mapping coronagraphs) with an inner working angle of  $3\lambda_0/D$ , that pointing offsets needed to be less than  $\pm 0.025 \lambda_0/D$  to limit the corresponding contrast degradation to  $2 \times 10^{-10}$  or less.

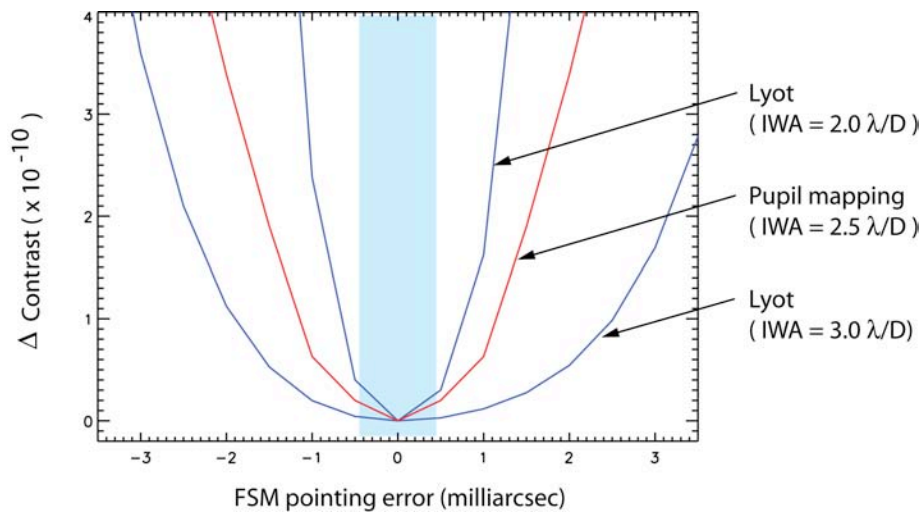


**Figure 3-1.** Delta contrast vs. fine steering mirror pointing errors, taken from the ACCESS final report (Trauger et al. 2009). Contrast degradations for representative coronagraphs are shown, for inner working angles of 3.0, 2.5, and 2.0  $\lambda_0/D$  (for  $\lambda_0 = 550 \text{ nm}$ ). Blue-shaded region indicates the  $\pm 0.45$  milliarcsec  $3\sigma$  pointing control limits estimated in the ACCESS pointing control study.

In the context of the laboratory testbed, this contrast degradation vs. pointing error corresponds to a drift (following a cycle of speckle nulling, and prior to further wavefront corrections) of the star image relative to the center of the Lyot occulting mask. Scaled to the HCIT, a  $\pm 0.025 \lambda_0/D$  pointing requirement corresponds to the stabilization of the occulting mask on the “star” within  $0.025 * 0.8 \mu\text{m} * 1500/30 = 1.0 \mu\text{m}$ , or about  $1.0 * 3/13 = 0.23$  pixel when projected to the CCD focal plane. This corresponds to a requirement on the drift in relative positions of the star and occulting mask as measured at the CCD focal plane. Note that the pointing control system in the ACCESS mission concept would provide active  $3\sigma$  stabilization of the star that is a factor of 5 better than  $\pm 0.025 \lambda_0/D$ , as would be required for a coronagraph operating with a smaller inner working angle of  $2 \lambda_0/D$ .

The milestone demonstration depends on the passive stability of the testbed. In practice,

the HCIT often exhibits larger motions than expected in the space environment. Figure 3-2 illustrates stability data recorded over a typical month during ACCESS coronagraph experiments in 2008. As noted in the caption, the configuration was not identical to the testbed layout for this milestone, but will serve to illustrate the nature of the drifts during one of the most recent experiment runs with the Lyot table in a stable HCIT vacuum environment.

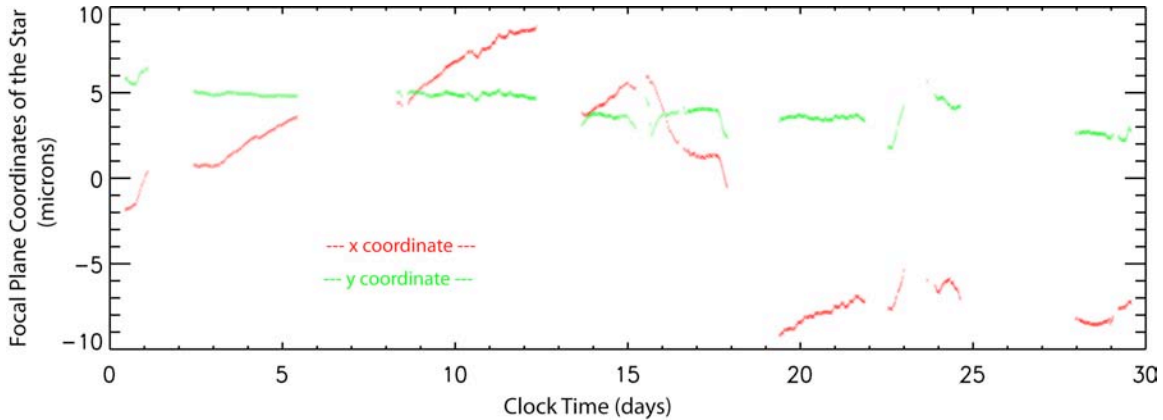


**Figure 3-2.** *Drift in the position of the HCIT “star” as measured at the CCD focal plane, for a typical month (Oct 6 – Nov 5, 2008). The HCIT configuration differed from the current configuration in one main respect: the focal lengths for M1 and M2 were 774 mm, rather than the current 1500 mm. The source of the drifts is not known with certainty, and the current testbed configuration may prove to be more (or less) stable due to changes in the configuration and opto-mechanical mounts. Gaps in the streams of data are periods of downtime on the HCIT.*

Past experience with a coronagraph with a  $3 \lambda_0/D$  inner working angle, the Lyot coronagraph demonstration for ACCESS in February 2009, showed that the nulling procedure was able to compensate for the x-coordinate drift only when it was less than  $1 \mu\text{m}$  per day. As seen in the figure, the HCIT systems were up and operating, with measured drifts in the x-coordinate of  $\pm 1 \mu\text{m}$  per day or better, for about half of the clock time during the month.

We take three conclusions from these data. (1) Past experience indicates that HCIT has typically operated at the required level of stability for about half the clock time. (2) While the stability of the testbed, in the current configuration and in this year’s HCIT vacuum environment, will not be known with certainty until the milestone demonstration has been underway in vacuum for a few weeks, it is clear that measures to improve stability and/or minimize testbed computer/software/mechanism downtime are critical for the success of TDEM experiments. (3) Future milestone demonstrations with working angles smaller than  $3 \lambda_0/D$  will benefit from further improvements in testbed stability.

## 9. Appendix 3 – Overview of the ACCESS concept

A brief overview of the ACCESS mission concept is attached. It was prepared for the September 2009 “Pathways towards Habitable Planets” conference in Barcelona, to appear in the corresponding ASP Conference Series. The hybrid Lyot technology milestone demonstration is one element in the developmental readiness for such a probe-class exoplanet mission.

## ACCESS: A Concept Study for the Direct Imaging and Spectroscopy of Exoplanetary Systems

J. Trauger,<sup>1</sup> K. Stapelfeldt,<sup>1</sup> W. Traub,<sup>1</sup> J. Krist,<sup>1</sup> D. Moody,<sup>1</sup>  
E. Serabyn,<sup>1</sup> D. Mawet,<sup>1</sup> L. Pueyo,<sup>1</sup> S. Shaklan,<sup>1</sup> C. Henry,<sup>1</sup> P. Park,<sup>1</sup>  
R. Gappinger,<sup>1</sup> P. Brugarolas,<sup>1</sup> J. Alexander,<sup>1</sup> V. Mireles,<sup>1</sup> O. Dawson,<sup>1</sup>  
O. Guyon,<sup>2,3</sup> J. Kasdin,<sup>4</sup> B. Vanderbei,<sup>4</sup> D. Spergel,<sup>4</sup> R. Belikov,<sup>5</sup>  
G. Marcy,<sup>6</sup> R.A. Brown,<sup>7</sup> J. Schneider,<sup>8</sup> B. Woodgate,<sup>9</sup> G. Matthews,<sup>10</sup>  
R. Egerman,<sup>10</sup> P. Voyer,<sup>10</sup> P. Vallone,<sup>10</sup> J. Elias,<sup>10</sup> Y. Conturie,<sup>10</sup>  
R. Polidan,<sup>11</sup> C. Lillie,<sup>11</sup> C. Spittler,<sup>11</sup> D. Lee,<sup>11</sup> R. Hejal,<sup>11</sup>  
A. Bronowick,<sup>11</sup> N. Saldivar,<sup>11</sup> M. Ealey,<sup>12</sup> and T. Price<sup>12</sup>

**Abstract.** ACCESS is one of four medium-class mission concepts selected for study in 2008/9 by NASA's Astrophysics Strategic Mission Concepts Study program. In a nutshell, ACCESS evaluates a space telescope designed for extreme high-contrast imaging and spectroscopy of exoplanetary systems. An actively-corrected coronagraph is used to suppress the glare of diffracted and scattered starlight to the levels required for exoplanet imaging. The ACCESS study asks: What is the most capable medium-class coronagraphic mission that is possible with telescope, instrument, and spacecraft technologies available today?

### 1. Overview

Our science objective is the direct observation of exoplanetary systems, possibly dynamically full, that harbor exoplanets, planetesimals, and dust/debris structures. Direct coronagraphic imaging at visible (450–900 nm) wavelengths and low-resolution ( $R=20$ ) spectroscopy of exoplanet systems in reflected starlight enables a broad science program that includes a census of nearby known RV planets in orbits beyond  $\sim 1$  AU; a search for mature exoplanet systems beyond the RV survey limits including giant planets, super-earths, and possibly a dozen earth-mass planets; observations of debris structures as indicators of unseen

---

<sup>1</sup>Jet Propulsion Laboratory, Caltech, Pasadena, CA, USA

<sup>2</sup>Subaru Telescope, Hilo, HI, US

<sup>3</sup>University of Arizona, Tucson, AZ, USA

<sup>4</sup>Princeton University, Princeton, NJ, USA

<sup>5</sup>NASA Ames Research Center, Moffett Field, CA, USA

<sup>6</sup>University of California, Berkeley, CA, USA

<sup>7</sup>Space Telescope Science Institute, Baltimore, MD, USA

<sup>8</sup>Paris Observatory, Meudon, France

<sup>9</sup>NASA Goddard Space Flight Center, Greenbelt, MD, USA

<sup>10</sup>ITT Space Systems Division, Rochester, NY, USA

<sup>11</sup>Northrop Grumman Corporation, Redondo Beach, CA, USA

<sup>12</sup>Northrop Grumman Xinetics, Devens, MA, USA

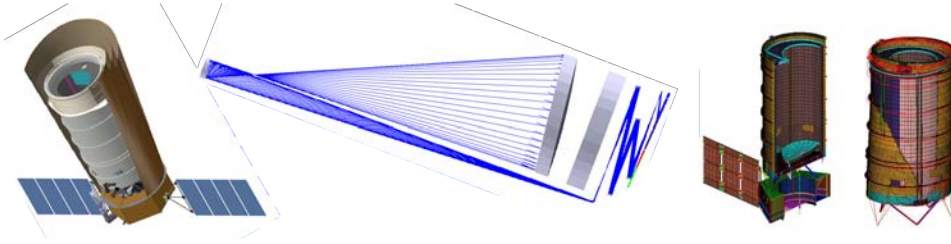


Figure 1. The ACCESS observatory, an actively corrected coronagraphic space telescope for the study of exoplanetary systems.

planets and planetesimals; and imaging of dust structures in circumstellar environments as a probe of the life cycle of planetary systems from young stellar objects to proto-planetary nebulae.

The ACCESS study compares the performance and readiness of four major coronagraph architectures. ACCESS defines a conceptual space observatory platform as the “level playing field” for comparisons among coronagraph types. And it uses laboratory validation of four representative coronagraph types as a second “level playing field” for assessing coronagraph hardware readiness. The “external occulter” coronagraph is not considered here, on the presumption that a concept requiring two spacecraft is beyond the bounds of a medium-class mission. ACCESS identifies a genre of scientifically compelling mission concepts built upon mature subsystem technologies, and evaluates science reach of a medium-class coronagraph mission.

## 2. Performance Assessment

The observatory architecture represents the “best available” for exoplanet coronagraphy within the scope (cost, risk, schedule) of a NASA medium-class mission. Visible wavelengths (450–900 nm) are selected for a minimum inner working angle (IWA). All coronagraphs require an observatory system with exceptional pointing control and optical stability, with deformable mirrors (DMs) for active wavefront control. ACCESS requires systems with high technology readiness (near or above TRL6) for reliable estimates of science capabilities and reliable determinations of cost and schedule. The baseline observatory architecture defines a capable platform for meaningful comparisons among coronagraph types.

The ACCESS observatory (Figure 1) is comprised of a Gregorian telescope with an unobscured 1.5 meter diameter aperture, end-to-end system design for alignment stability, thermal isolation of the telescope secondary mirror and all downstream optics, a precision pointing control system, and an actively-corrected coronagraph for the suppression of diffracted and scattered light. The observatory orbits at L2 halo for a baseline mission of five years.

High-order wavefront control is provided by a pair of deformable mirrors. The evolution of precision deformable mirrors based on monolithic PMN electroceramic actuator arrays is illustrated in Figure 2. Mirror facesheets are fused silica, with surfaces polished nominally to  $\lambda/100$  rms. Surface figure is settable and stable (open loop) to 0.01 nm rms over periods of 6 hours or more in a



Figure 2. The development of the monolithic PMN deformable mirrors. From left to right: a  $32 \times 32$  mm array (1024 actuators), of the type used for all HCIT demonstrations to date; a  $64 \times 64$  mm array (4096 actuators) first installed on HCIT in 2009; a  $48 \times 48$  mm array (2304 actuators) to be used to demonstrate TRL6 flight-readiness; and the  $48 \times 48$  array on the JPL shake table.

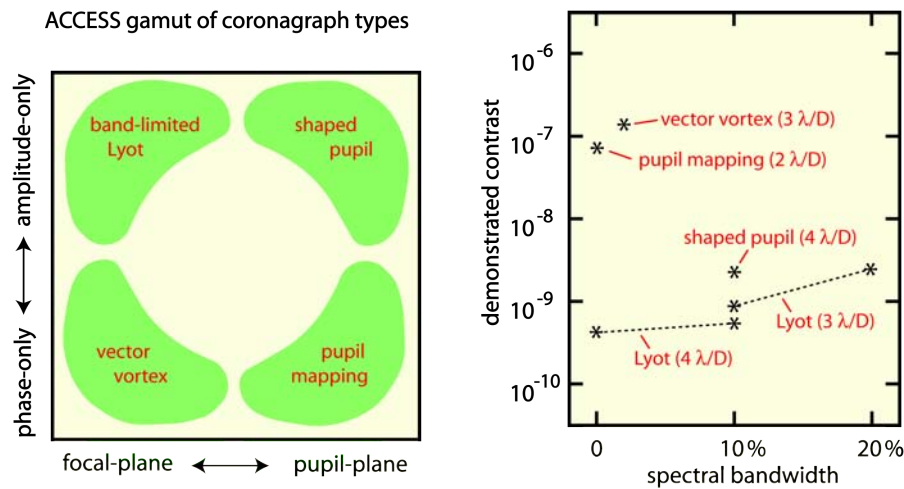


Figure 3. *Left:* The coronagraph types in the ACCESS study. *Right:* The best contrast demonstrated in the laboratory to date (September 2009) (see text for details).

vacuum testbed environment. All DMs have been manufactured and delivered to JPL by Xinetics Inc.

The gamut of coronagraph types in the ACCESS study is indicated in Figure 3 (at left). The four major coronagraph types perform starlight rejection with combinations of phase and amplitude elements placed in focal and pupil planes.

The best demonstrated laboratory contrast to date (September 2009) for each type is plotted in Figure 3 (at right), as follows. Lyot data at  $4\lambda/D$  are TPF performance milestones demonstrated on the High Contrast Imaging Testbed (HCIT) (Trauger et al. 2006, 2007; Kern et al. 2008) with band limited masks (Kuchner & Traub 2002). Lyot data at  $3\lambda/D$  were achieved on the HCIT in the course of the ACCESS study with hybrid Lyot masks (Moody et al. 2008). Shaped pupil (Spergel 2000) data were obtained on the HCIT with masks designed at Princeton (Belikov et al. 2004). Vortex result was demonstrated on

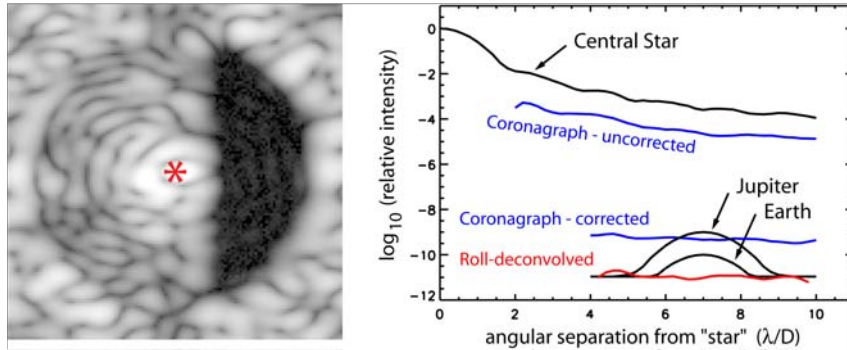


Figure 4. *Left:* The high-contrast dark field (D-shaped) created by a single DM in the laboratory experiments. *Right:* A comparison of the azimuthally averaged PSFs of (a) the star with focal plane mask offset and Lyot stop in place; (b) the coronagraph field with all DM actuators set to equal voltages; (c) the coronagraph with DM set for a dark half-field and (d) the result of simulated roll deconvolution with the set of 480 consecutive coronagraph images. PSFs of a nominal Earth and Jupiter are also indicated (Trauger & Traub 2007).

the HCIT during the ACCESS study with a vector vortex mask (Mawet et al. 2010). The result for pupil mapping (Guyon et al. 2006) came from the new Ames testbed (Belikov et al. 2009). We note that post-observation data processing methods can be expected to improve the threshold for exoplanet detection by an order of magnitude compared to the raw contrast values plotted in Figure 3, for all coronagraph types, and as illustrated in Figure 4 for the case of a Lyot coronagraph. We further note that significant improvements are expected in the coming months and years as an outcome of active laboratory developments with well-understood technologies.

Coronagraph contrast and stability have been demonstrated in the laboratory at the levels required to detect exoplanets. Figure 4 shows the high-contrast dark field (D-shaped) created by a single DM in laboratory experiments (a pair of DMs clears a full, two-sided dark field). At right in the figure is a comparison of azimuthally averaged PSFs of (a) the star, with focal plane mask offset and Lyot stop in place; (b) the coronagraph field with the DM set to a flat surface figure; (c) the coronagraph with DM set for a dark half-field; and (d) the result of simulated roll deconvolution with the set of 480 consecutive coronagraph images. PSFs of a nominal Earth and Jupiter are also indicated (Trauger & Traub 2007).

Structural and thermal models guide the observatory design and inform the optical performance models with estimates of structure dynamics, vibration isolation, pointing control, thermal gradients across the primary mirror and forward metering structures, alignment drift in response to telescope slews and roll.

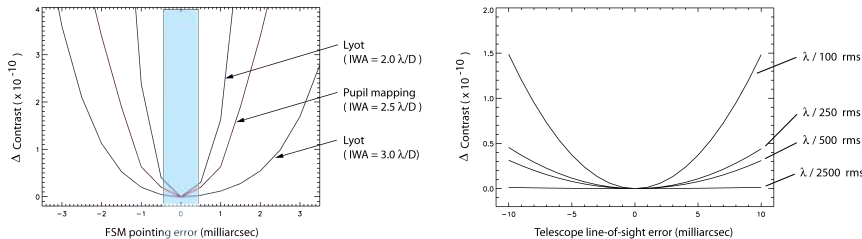


Figure 5. *Left:* Contrast deltas at the IWA for representative coronagraphs designed for 2.0, 2.5 and 3.0  $\lambda/D$ . *Right:* Contrast deltas (vs. rms surface figure of the optical elements following the primary mirror) due to beamwalk on the optics upstream of the fine steering mirror.

Telescope body pointing (i.e., line of sight) is stabilized to 1 milliarcsec ( $3\sigma$ ) with an active jitter control system. Figure 5 shows the contrast deltas (vs. rms surface figure of the optical elements following the primary mirror) due to beamwalk on the optics upstream of the fine steering mirror. The telescope attitude control system, augmented by a fine steering mirror within the coronagraph, stabilizes the star image on the coronagraph occulting mask (all four coronagraphs have an occulting mask) to 0.45 milliarcsec ( $3\sigma$ ), as required for high contrast at inner working angles as small as 2  $\lambda/D$  (Figure 5).

### 3. Science Program

A baseline minimum science mission has been developed in terms of end-to-end optical models (e.g., Krist 2007) that incorporate the baseline observatory architecture and laboratory-validated estimates of coronagraph performance. A number of results are collected here.

Figure 6 depicts the ACCESS discovery space, which lies above the labeled curve at lower right in the diagram. A 1.5 meter coronagraph in space offers significant contrast advantages over even the largest current and future observatories on the ground.

Figure 7 gives two representations of the completeness in an ACCESS survey for exoplanets. At left are the detections of Jupiter-twins within  $45^\circ$  of elongation from their parent stars, to  $S/N = 10$ , using the ACCESS Lyot coronagraph with an IWA = 2  $\lambda/D$  for a number of integration times. Note that the probability that an exoplanet will have a star-planet separation greater than that at  $45^\circ$  elongation is 50% or more. At right, the number of planets, in four mass categories, detectable to  $S/N = 10$  in integration times of one day or less, using the ACCESS Lyot coronagraph with an IWA = 2.5  $\lambda/D$ .

Figure 8 tabulates of the number of nearby stars that could be searched with various ACCESS coronagraphs to the depth of  $10\text{-}\sigma$  detections of Jupiter twins in each of six visits to the star over a period of 2.5 years. The row indicated by the arrow is an estimate based on coronagraph performance demonstrated in the laboratory at 3.0  $\lambda/D$  with the Lyot coronagraph. The other rows represent coronagraph performance that may be achieved with further development of known technologies in the near future. The column for  $45^\circ$  from maximum

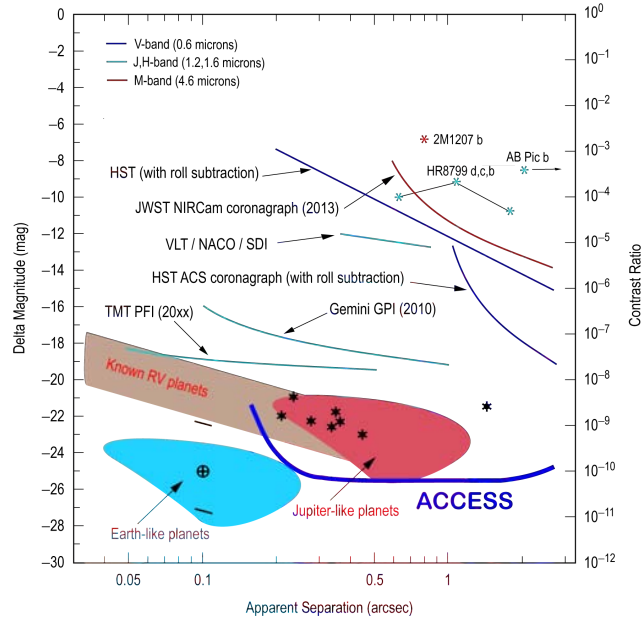


Figure 6. The ACCESS discovery space. Sensitivity for exoplanet detections is compared with current and future observatories in terms of brightness relative to the central star vs. apparent separation. Known exoplanets are shown as asterisks. Shaded areas indicate the regions of high probability of detecting planets orbiting the nearest 100 AFGK stars (for Jupiter-twins in 5AU orbits and Earth-twins in 1 AU orbits, respectively). The detection range for ACCESS is the area above the bold curve at bottom right.

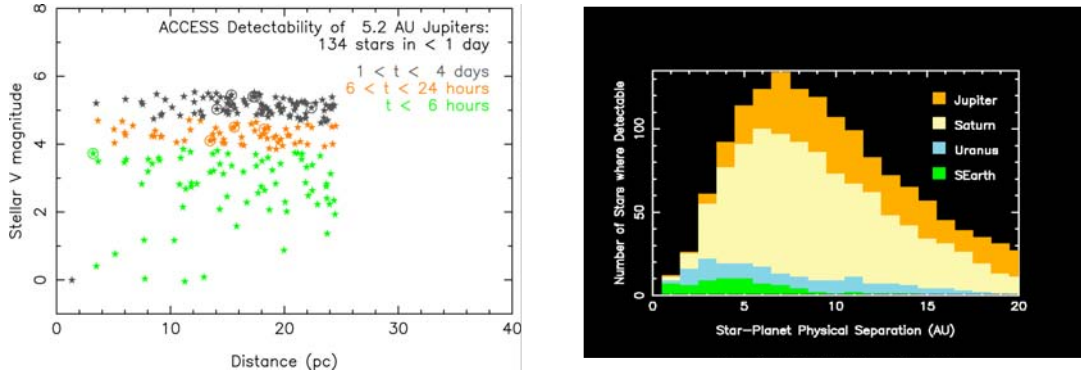


Figure 7. Two representations of the completeness in an ACCESS survey for exoplanets. *Left:* Detections of Jupiter-twins within  $45^\circ$  of elongation from their parent stars to  $S/N = 10$ , using the ACCESS Lyot coronagraph with an IWA =  $2 \lambda/D$  for a number of integration times. *Left:* The number of planets, in four mass categories, detectable to  $S/N = 10$  in integration times of one day or less using the ACCESS Lyot coronagraph with an IWA of  $2.5 \lambda/D$ .

Table 1: Number of nearby stars that can be surveyed for 5.2 AU Jupiters, IWA 3.0  $\lambda/D$ 

Coronagraph Type	Planet 45° from max elong	Planet 15° from max elong
Lyot	117	175
PIAA	166	278
Vortex	135	204

Table 2: Number of nearby stars that can be surveyed for 5.2 AU Jupiters, IWA 2.5  $\lambda/D$ 

Coronagraph Type	Planet 45° from max elong	Planet 15° from max elong
Lyot	153	218
PIAA	178	267
Vortex	154	228

Table 3: Number of nearby stars that can be surveyed for 5.2 AU Jupiters, IWA 2.0  $\lambda/D$ 

Coronagraph Type	Planet 45° from max elong	Planet 15° from max elong
Lyot	170	230
Vortex	164	241

Note: Accurate PIAA wavefront control solution not available for IWA = 2.0  $\lambda/D$

Figure 8. The number of nearby stars that could be searched with various ACCESS coronagraphs to the depth of 10- $\sigma$  detections of Jupiter-twins in each of six visits to the star over a period of 2.5 years. The arrow corresponds to the ACCESS minimum science program based on current demonstrated technologies. Ongoing developments are expected to bring the demonstrated readiness of other coronagraph configurations to the search sensitivities shown in the table.

elongation corresponds to an observational completeness of 50% or more in each visit, approaching 100% after six epochs spread over several years.

#### 4. Summary

The ACCESS study has considered the relative merits and readiness of four major coronagraph types, and hybrid combinations, in the context of a conceptual medium class space observatory.

**Using demonstrated high-TRL technologies, the ACCESS minimum science program surveys the nearest 120+ AFGK stars for exoplanet systems, and surveys the majority of those for exozodiacal dust to the level of 1 zodi at 3 AU. Discoveries are followed up with R=20 spectrophotometry.**

Ongoing technology development and demonstrations in the coming year are expected to further enhance the science reach of an ACCESS mission, in advance of a NASA AO for a medium class mission. The study also identifies areas of technology development that would advance the readiness of all major coronagraph types in the coming 5 years.

**Acknowledgments.** The research described in this paper was carried out at the Jet Propulsion Laboratory, California Institute of Technology, under a contract with the National Aeronautics and Space Administration.

#### References

- Belikov, R., et al. 2009, Proc. SPIE, 7440, 74400J  
 Belikov, R., Kasdin, N.J., & Vanderbei, R.J. 2006, ApJ, 652, 833  
 Giveón, A., et al. 2007, Proc. SPIE, 6691, 66910A  
 Guyon, O., et al. 2005, ApJ, 622, 744

- Guyon, O., et al. 2008, Proc. SPIE, 7010, 7010–66  
Kern, B., et al. 2008, JPL Document D-60951  
Krist, J.E. 2007, Proc. SPIE, 6675, 66750P  
Kuchner, M.J., and Traub, W.A. 2002, ApJ, 570, 900  
Mawet, D., et al. 2010, ApJ, 709, 53  
Moody, D., Gordon, B., & Trauger, J. 2008, Proc. SPIE, 7010, 7010–81  
Spergel, D.N. 2000, Astro-ph/0101142  
Trauger, J., et al. 2006, JPL Document D-35484  
Trauger, J., et al. 2007, Proc. SPIE, 6693, 66930X  
Trauger, J.T., and Traub, W.A. 2007, Nature, 446, 771  
Trauger, J., et al. 2009, ACCESS final report to NASA (copies available on request)